IEEE Access
Multidisciplinary | Rapid Review | Open Access Journal

Received June 12, 2017, accepted July 31, 2017, date of publication August 4, 2017, date of current version September 6, 2017.

Digital Object Identifier 10.1109/ACCESS.2017.2735994

Multidimensional OAM-Based Secure High-Speed Wireless Communications

IVAN B. DJORDJEVIC, (Senior Member, IEEE)
Department of Electrical and Computer Engineering, College of Engineering, The University of Arizona, Tucson, AZ 85721, USA
College of Optical Sciences, The University of Arizona, Tucson, AZ 85721, USA
Corresponding author: Ivan B. Djordjevic (e-mail: ivan@email.arizona.edu).

ABSTRACT To address key challenges for beyond 5G wireless technologies in a simultaneous manner, we propose an orbital angular momentum (OAM)-based, secure, energy-efficient multidimensional coded modulation. The key idea is to employ all available degrees of freedom (DOFs) to convey the information over the wireless links, including amplitude, phase, polarization state, and spatial-domain DOFs. In particular, the OAM is associated with the azimuthal phase dependence of the wavefront, and represents an underutilized DOF. Given that OAM eigenstates are orthogonal, an arbitrary number of bits per symbol can be transmitted. Here, we propose utilizing OAM DOF not only to improve spectral and energy efficiencies, but also to significantly improve the physical-layer security of future wireless networks. To implement the OAM multiplexer and demultiplexer in the RF domain, we propose using properly designed antenna arrays. We also propose employing the Slepian sequences as either basis functions in baseband or impulse responses of antenna arrays in passband to further increase the dimensionality of the wireless system and enable beyond 1-Tb/s wireless transmission. Monte Carlo simulations demonstrate high tolerance to fading effects of LDPC-coded multidimensional signaling schemes compared with the conventional LDPC-coded QAM.

INDEX TERMS Coded modulation, forward error correction, physical-layer security, low-density parity-check codes, multidimensional signaling, OAM antennas, wireless communications.

I. INTRODUCTION

The key challenges for beyond 5G wireless technologies include limited wireless bandwidth infrastructure; insufficient energy-, cost-, and resource-efficiencies; inadequate security, insufficient spectrum efficiency, heterogeneity of network segments, high traffic demands, the existence of various cell sizes (small cells), interference management, and introduction of intelligence. Moreover, the 5G will be user-centric driven instead of service-centric 4G [1]–[5]. We anticipate that beyond 5G networks, supported by optical access networks [6], should be able provide an open communication platform to integrate cellular systems, satellite systems, data centers, business/home gates, and any future open and cloud networks. However, these goals are impossible to achieve with currently existing both wireless and optical networks technologies. It is, therefore, necessary to make a dramatic improvement in the wireless spectrum and energy efficiencies in order to cope with the incoming bandwidth capacity crunch. Moreover, the security in existing wireless networks is not sufficiently good. To address these key challenges for future beyond 5G wireless technologies in a simultaneous manner, in this paper we propose an orbital angular momentum (OAM)-based, secure, energy-efficient high-speed coded-modulation scheme enabling future wireless communications.

Although there are many proposals on how to deal with the incoming network bandwidth capacity crunch in the optical domain [7]–[13], the security of both optical and wireless networks have not been adequately addressed. By taping out the portion of either optical or wireless signals, the huge amount of data can be compromised. On the other hand, todays security of either optical or wireless networks relies on the computational difficulty of reversing the one-way functions, and in principle cannot provide any indication of Eve's presence at any point in the communication process. Therefore, the security of wireless networks is becoming one of the major issues to be addressed sooner rather than later. To address the security issues of future wireless networks, the following strategy has been proposed. It is well known that we can associate with a photon both spin angular momentum (SAM), related to polarization; and OAM, related to azimuthal dependence of the wavefront, as shown in [14]–[24].

On the hand, related to wireless communications, in series of papers [25]–[30], it has been shown that OAM can be generated in the RF domain as well, by employing circular array antennas, circular traveling-wave antennas, helical parabolic antennas, spiral phase plates, to mention few. The OAM degree of freedom (DOF) has been used mostly to improve the spectral efficiencies. However, because the OAM eigenstates are orthogonal, this underutilized DOF can also be employed to improve the physical-layer security (PLS) in wireless networks. We have recently shown that the aggregate secrecy capacity, defined as the total capacity that Eve cannot obtain any meaningful information, can be improved by using OAM multiplexing [23], [24]. Therefore, the OAM DOF is proposed to increase the throughput and improve the security of wireless networks in a simultaneous manner.

From our previous multidimensional studies, related to optical communications, [7]–[13], we have concluded that the spectral efficiency in multidimensional signaling scheme is a linear function of number of dimensions, rather than only logarithmic in signal-to-noise ratio (SNR). Therefore, through multidimensional coded modulation, the spectral efficiency of existing wireless communication systems can be dramatically improved. However, these multidimensional signal constellation designs do not take energy-efficiency into account. Energy-efficient multidimensional coded modulation can be achieved through proper signal constellation design, which takes the energy constraint into account. The energy-efficient signal constellation design algorithm, to be described later, will be employed to perform this design efficiently.

The contributions of this paper can be summarized as follows. Firstly, a multidimensional-coded modulation scheme is proposed capable of solving the challenges of future beyond 5G wireless technologies. Secondly, we propose to use all available DOFs to convey the information over the wireless links including amplitude, phase, polarization state, and spatial-domain DOFs. In particular, the OAM is associated with azimuthal phase dependence of the wavefront, and represents an underutilized DOF. Because OAM modes are mutually orthogonal, an arbitrary number of bits per symbol duration can be transmitted. The OAM can also be combined with traditional MIMO approaches to further increase the aggregate data rate. Thirdly, we propose to utilize OAM modes not only to improve spectral- and energy-efficiencies, but also to significantly improve the physical-layer security of wireless networks. Fourthly, we propose to use the antenna array as an OAM multiplexer/demultiplexer. So far the antenna array is used to impose a single OAM mode, here we propose to use one antenna array to impose all desired OAM modes. Fifthly, we proposed an OAM-based encryption scheme suitable for wireless communications. Sixthly, we propose an energy-efficient signal constellation design algorithm suitable for wireless communications. Seventhly, we propose to utilize Slepian sequences as either discrete-time domain baseband basis functions or passband impulse responses of properly designed antenna arrays, thus representing a new DOF. Further, a digital hierarchy is proposed enabling multi-Tb/s wireless transmission. Finally, the OAM-based multidimensional PLS scheme is proposed with a potential of significantly improving the PLS of wireless networks.

The paper is organized as follows. In Section II, we describe the antenna arrays suitable for implementation of OAM multiplexer and demultiplexer. In the same section, an OAM-based encryption scheme suitable for wireless communication applications is described as well. Section III is devoted to description of the proposed software-defined, energy-efficient multidimensional coded modulation for the next generation of wireless communication systems. In the same section, an energy-efficient signal constellation design algorithm is described suitable for use in proposed multidimensional coded modulation. The digital hierarchy enabling multi-Tb/s wireless transmission is described as well. In Section IV, we describe the OAM-based physical layer security scheme that can potentially significantly improve secrecy capacities. The illustrative numerical results, demonstrating high potential of the proposed secure OAM-based multidimensional coded-modulation scheme, are provided in Section V. Some important concluding remarks are provided in Section VI.

II. ANTENNA ARRAYS SUITABLE FOR WIRELESS OAM MULTIPLEXING/DEMULTIPLEXING AND OAM-BASED ENCRYPTION

The angular momentum, $\boldsymbol{J}$, of the classical electromagnetic field can be written as [7]

$$\boldsymbol{J} = \frac{1}{4\pi c}\int_V \boldsymbol{E}\times\boldsymbol{A}dV + \frac{1}{4\pi c} \times \int_V \sum\nolimits_{k=x,y,z} E_k\,(\boldsymbol{r}\times\boldsymbol{\nabla})\,A_k dV, \quad (1)$$

where $\boldsymbol{E}$ is the electric field intensity, $\boldsymbol{A}$ is the vector potential, and c is the speed of light. The vector $\boldsymbol{A}$ is related to the magnetic field intensity $\boldsymbol{H}$ by $\boldsymbol{H} = \nabla\times\boldsymbol{A}$, and to the electric field intensity by $\boldsymbol{E} = -c^{-1}\partial\boldsymbol{A}/\partial t$. The second term in Eqn. (1) is identified as the OAM due to the presence of the *angular momentum operator* $\hat{\mathbf{L}} = -j(\boldsymbol{r}\times\boldsymbol{\nabla})$. Regarding optical communications, among various optical beams that can carry OAM, the *Laguerre-Gaussian* (LG) vortex beams can easily be implemented with the help of spatial light modulators [19]. The field distribution of the LG beam traveling along the z-axis can be expressed in cylindrical coordinates $[\rho, \phi, z]$ (ρ denotes the radial distance from propagation axis, ϕ denotes the azimuthal angle, and z denotes the propagation distance) as [20]–[22]:

$$u_{m,p}(\rho,\phi,z) = \sqrt{\frac{2p!}{\pi(p+|m|)!}}\frac{1}{w(z)}\left[\frac{\rho\sqrt{2}}{w(z)}\right]^{|m|} L_p^m\left(\frac{2\rho^2}{w^2(z)}\right) \cdot e^{-\frac{\rho^2}{w^2(z)}} e^{-\frac{jk\rho^2 z}{2(z^2+z_R^2)}} e^{j(2p+|m|+1)\tan^{-1}\frac{z}{z_R}} e^{-jm\phi}, \quad (2)$$

where $w(z) = w_0[1+(z/z_R)^2]^{1/2}$ (w_0 is the zero-order Gaussian radius at the waist), $z_R = \pi w_0^2/\lambda$ is the Rayleigh range (with λ being the wavelength), $k = 2\pi/\lambda$ is the propagation constant, and $L_p^m(\cdot)$ is the associated Laguerre polynomial, with p and m representing the radial and angular mode numbers, respectively. It can be seen from Eqn. (2) that the m-th mode of the LG beam has the azimuthal angular dependence in the form $\exp(-jm\phi)$, and consequently, the parameter m is also known as the azimuthal mode number (index). For $m = 0$, $u(\rho, \phi, z)$ becomes a zero-order Gaussian beam that presents the TEM_{00} mode. For $p = 0$, it is $L_p^m(\cdot) = 1$ for all m's, so that the intensity of an LG mode presents a ring of the radius proportional to $|m|^{1/2}$. It can be shown that for a fixed p, the following principle of orthogonality is satisfied:

$$\langle u_{m,p}|u_{n,p}\rangle = \int u_{m,p}^*(\rho,\phi,z)\, u_{n,p}(\rho,\phi,z)\, \rho d\rho d\phi = \delta_{nm}\int |u_{m,p}|^2 \rho d\rho d\phi \quad (3)$$

Therefore, different "OAM states" corresponding to a fixed p are all mutually orthogonal. The orbital momentum of a beam is proportional to the number of turns that propagation vector completes around the beam's axis after propagating a distance equal to one wavelength.

The orthogonality principle is also satisfied for pure OAM basis functions, defined as $\phi_n = \exp(jn\phi)$; $n = 0, \pm 1, \pm 2, \cdots$, because

$$\langle \phi_m|\phi_n\rangle = \frac{1}{2\pi}\int_0^{2\pi} e^{-jm\phi}e^{jn\phi}d\phi = \begin{cases}1, & n=m\\ 0, & n\neq m\end{cases} = \delta_{nm} \quad (4)$$

Given that OAM-based basis functions are mutually orthogonal they can be used as the basis functions for multidimensional signaling [7]–[13] as well as to improve the PLS in optical/wireless networks [23], [24].

Regarding the generation of OAM modes for wireless applications, it has been recently shown that circular traveling-wave antenna [25], spiral parabolic antenna [26], dual mode antennas [27], and circular antenna arrays [28]–[30], to mention few, can be used to generate OAM modes in the RF domain. For instance, the circular traveling-wave antenna of radius a, with azimuthal dependence of current distribution $I = I_0 e^{jl\phi}$, based on [28]–[31], will generate the electromagnetic (EM) waves with the vector potential expressed in spherical coordinates $[r, \theta, \phi]$ as:

$$\begin{aligned}\mathbf{A}(\mathbf{r}) &= \frac{\mu_0 I_0}{4\pi}\oint_C e^{jl\phi}\frac{e^{jk|\mathbf{r}-\mathbf{r}'|}}{|\boldsymbol{r}-\boldsymbol{r}'|}\mathrm{d}l'\\ &\cong \frac{(-j)^{-l}a}{r}\frac{\mu_0 I_0 e^{jkr}}{4}e^{jl\phi}J_{l-1}(ka\sin\theta)\\ &\quad\times\left[\sin\theta\hat{\mathbf{r}}+\cos\theta\hat{\theta}+j\hat{\phi}\right]\\ &\quad+\frac{(-j)^{-l}a}{r}\frac{\mu_0 I_0 e^{jkr}}{4}e^{jl\phi}J_{l+1}(ka\sin\theta)\\ &\quad\times\left[\sin\theta\hat{\mathbf{r}}+\cos\theta\hat{\theta}-j\hat{\phi}\right]\end{aligned} \quad (5)$$

where $k = 2\pi/\lambda$ is the wave number, C denotes the integration contour, $\boldsymbol{r}$ is the position vector, and $J_l(\cdot)$ is the Bessel function of the first kind and the l-th order. Clearly, the term $e^{jl\phi}$ corresponds to the azimuthal phase dependence of the l-th OAM mode of the vector potential. After substitution of Eqn. (5) into (1), because of the rotational symmetry only the angular momentum in the direction of propagation will survive the integration over the whole EM beam (wave), which can be expressed in cylindrical coordinates $[\rho, \phi, z]$ as follows:

$$L_z = \varepsilon_0\int_0^{2\pi} d\phi\iint \mathrm{Re}\left\{j\mathbf{E}^*\left(\hat{\mathbf{L}}\cdot\mathbf{A}\right)\right\}\rho d\rho dz, \quad (6)$$

where $\hat{\mathbf{L}}$ is the angular momentum operator introduced above, and $\boldsymbol{A}$ is the vector potential .

By segmenting this circular antenna into N segments, with each segment carrying the same RF signal but with an incremental phase shift of $2\pi n/N$, we can impose the n-th OAM mode on the RF carrier. Here we further propose to employ the *antenna arrays* to implement OAM multiplexer and OAM demultiplexer as follows.

A. GENERATION AND DETECTION OF OAM MODES IN THE RF DOMAIN BY ANTENNA ARRAYS

An antenna arrays consist of several antennas or antenna elements properly arranged in the space [31], [32]. Depending on the space arrangement of antenna elements, antenna arrays can be classified as linear array, circular array (in which antenna elements are arranged along a circular ring), planar array, and conformal array antennas. Clearly, the circular antenna arrays are very similar to segmented circular antenna discussed above. As an illustration, here we will show that even a linear antenna array, shown in Fig. 1, can be used to generate the OAM modes. For the transmit array antenna of identical elements, the radiation pattern can be found by applying the *pattern multiplication theorem* [31], claiming that the array pattern is the product of the array element pattern and the *array factor (AF)*. The AF is a function dependent only on the geometry of the antenna array and excitation of the elements. Since the array factor is independent of the antenna type, the isotropic radiators can be employed in the derivation of the AF. Inspired by this theorem, we will use the antenna array to perform the *OAM multiplexing*, instead of imposing a single OAM mode, which is common practice in the literature [25]–[30], with each element in the array being composed of an isotropic radiator element and spiral phase plate (SPP) to introduce the desired azimuthal phase shift as explained below. The field of an isotropic radiator located in the origin is given by:

$$E_\theta = \frac{I_0}{4\pi}\frac{e^{-jkr}}{r}, \quad (7)$$

where r is the distance of the observation point P from the origin, k is the wave number ($k = 2\pi/\lambda$) and I_0 is the current magnitude applied. Let us now observe the transmit $(2N+1)$-elements linear array shown in Fig. 1. The current complex

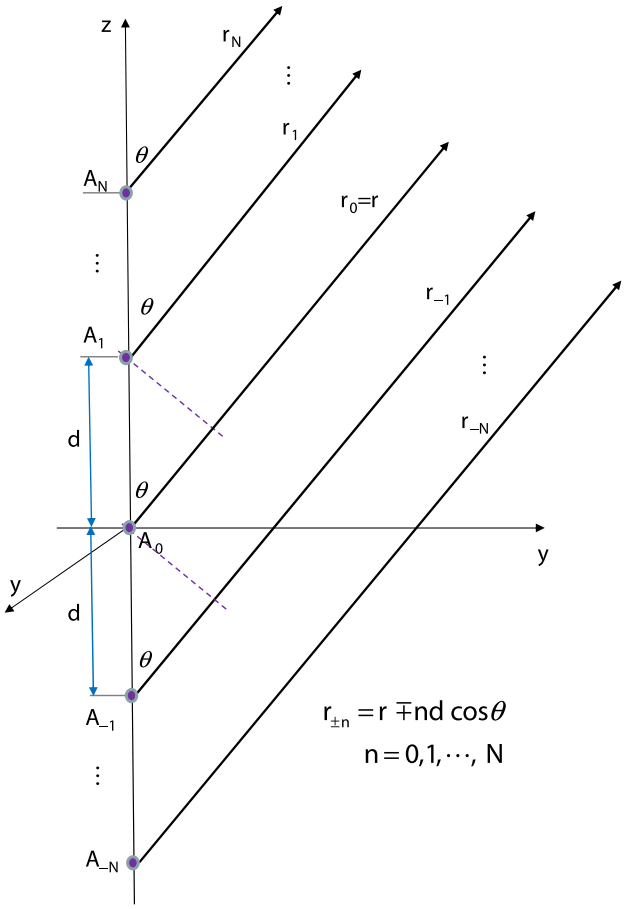

FIGURE 1. Transmit $(2N+1)$-elements linear array suitable for generation of OAM modes.

amplitude of the n-th array element is given by $I(n) = I_n e^{j\phi_n}$, where I_n denotes QAM symbol transmitted in a given symbol interval, as shown in Fig. 2(a), while ϕ_n is the phase shift with respect to the element placed in the origin.

Based on Fig. 1 we conclude that the far field for the n-th array element is given by:

$$E_{\theta,\pm n} \cong \frac{I_n e^{j\phi_{\pm n}}}{4\pi}\frac{e^{-jkr_n}}{r} = \frac{I_0 e^{j\phi_n}}{4\pi}\frac{e^{-jk[r\mp nd\cos\theta]}}{r}; \quad n = 0, 1, \cdots, N-1; \quad \phi_0 = 0. \tag{8}$$

The overall $(2N+1)$-elements array far field can be determined by the superposition principle:

$$E_\theta = \sum_{m=-N+1}^{N-1} E_{\theta,m} = \sum_{m=-N+1}^{N-1} \frac{I_m e^{j\phi_m}}{4\pi}\frac{e^{-jk[r-md\cos\theta]}}{r} = \underbrace{\frac{I_0}{4\pi}\frac{e^{-jkr}}{r}}_{E_{\theta,0}} \underbrace{\sum_{m=-N+1}^{N} \frac{I_m}{I_0} e^{j[\phi_m + mkd\cos\theta]}}_{AF}. \tag{9}$$

Clearly, when $I_m = I_0$, the second term represents the AF in a conventional linear array. Now by selecting the azimuthal phase shift in the m-th element to be $\phi_m = m\phi$, the Eqn. (9) can be re-written as follows:

$$E_\theta = \frac{1}{4\pi}\frac{e^{-jkr}}{r}\sum_{m=-N+1}^{N-1} I_m e^{jm\phi} e^{jkmd\cos\theta}. \tag{10}$$

The m-th component in Eqn. (10) contains the azimuthal phase term $\exp(jm\phi)$, indicating that the linear array from Fig. 1 represents an OAM multiplexer. The m-th transmit array antenna element can be implemented as an isotropic antenna integrated together with the SPP to introduce the azimuthal phase shift of $\phi_m = m\phi$, where ϕ is the azimuthal angle ranging from 0 to 2π The operation principle of such SPP has already been described in [30] (see Fig. 13.3 in that article and corresponding text), and can be fabricated with the help of 3-D nanoscribe printer. Namely, to introduce the m-th OAM mode we need to azimuthally vary the thickness of the plate as follows $h(m\phi) = m\phi\lambda/[2\pi(n-1)]$, where n is the refractive index of material and λ is the operating wavelength. Therefore, required azimuthally varied thickness of the SPP to introduce m-th OAM modes will be m times larger than that of OAM mode 1.

On receiver side, to detect the n-th OAM mode, the n-th element of receive antenna array is driven with the current complex magnitude $\exp(-jn\phi)$, so that the corresponding signal at the output the n-th antenna element is given by:

$$\begin{aligned}\frac{1}{2\pi}\int_0^{2\pi} e^{-jn\phi}E_\theta d\phi &= \frac{1}{2\pi}\int_0^{2\pi} e^{-jn\phi}\frac{e^{-jkr}}{4\pi r}\sum_{m=-N+1}^{N-1} I_m e^{jm\phi}e^{jkmd\cos\theta}d\phi \\ &= \frac{1}{4\pi}\frac{e^{-jkr}}{r}I_n e^{jknd\cos\theta},\end{aligned} \tag{11}$$

which is proportional to the transmitted symbol I_n on the n-th array element of transmit antenna array, and we have successfully converted the n-th OAM to the 0-th mode. Similarly to transmitter side, the n-th receiver antenna array element can also be implemented as an isotropic antenna integrated together with the spiral phase plate, which will now introduce the azimuthal phase shift of $-n\phi$. This phase plate will detect only the n-th OAM and reject the other OAM modes, effectively performing the action described by Eqn. (11).

It has been already demonstrated that circular antenna array can be used to generate a given OAM [29], [30]. The approach we proposed here is different, the antenna array is not used to generate a single OAM mode, but instead to perform OAM multiplexing and demultiplexing. The OAM antenna array element, shown in Fig. 2, is symbolically represented by a phase shifter to impose the OAM mode $\exp(jm\phi)$ and an antenna element. On receiver side, the n-th OAM array element in Fig. 2(b) is symbolically denoted by the receive antenna element followed by phase shifter and integrator to perform the projection along the n-th OAM basis function, as described by Eqn. (11). The configurations of RF and transmitter and receiver are the same as in Fig. 2. The corresponding schemes for wireless OAM

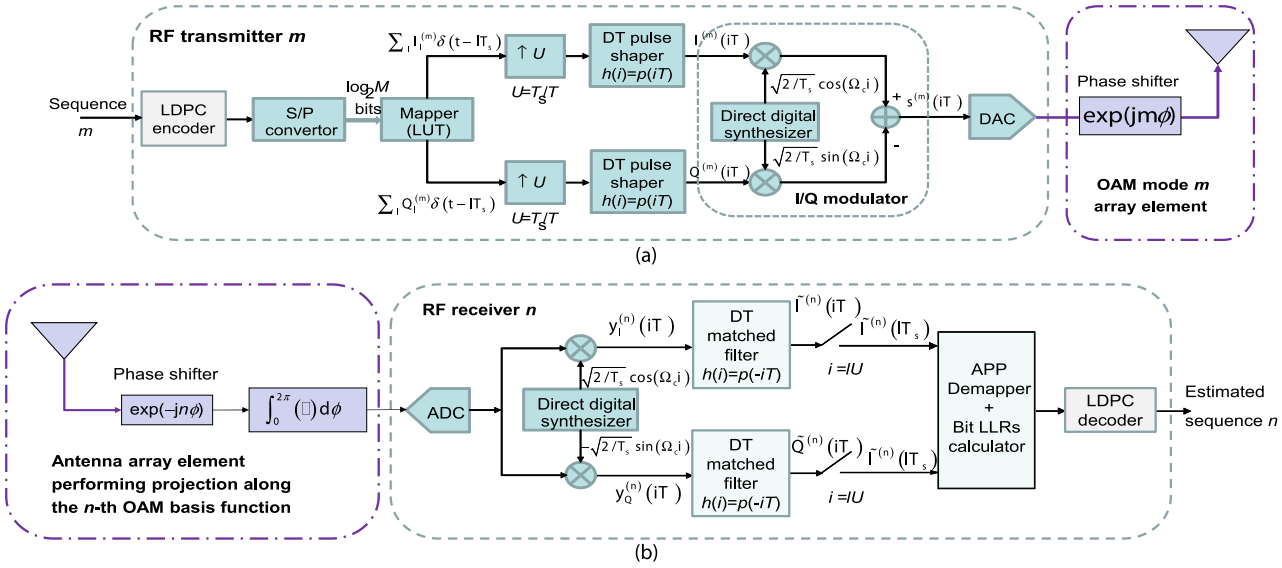

FIGURE 2. Software-defined RF transceiver configuration: (a) transmitter corresponding to the *m*-th OAM mode and (b) receiver corresponding to the *n*-th OAM mode. DT: discrete-time, DAC: digital-to-analog converter, ADC: analog-to-digital converter, APP: *a posteriori* probability, LLR: log-likelihood ratio.

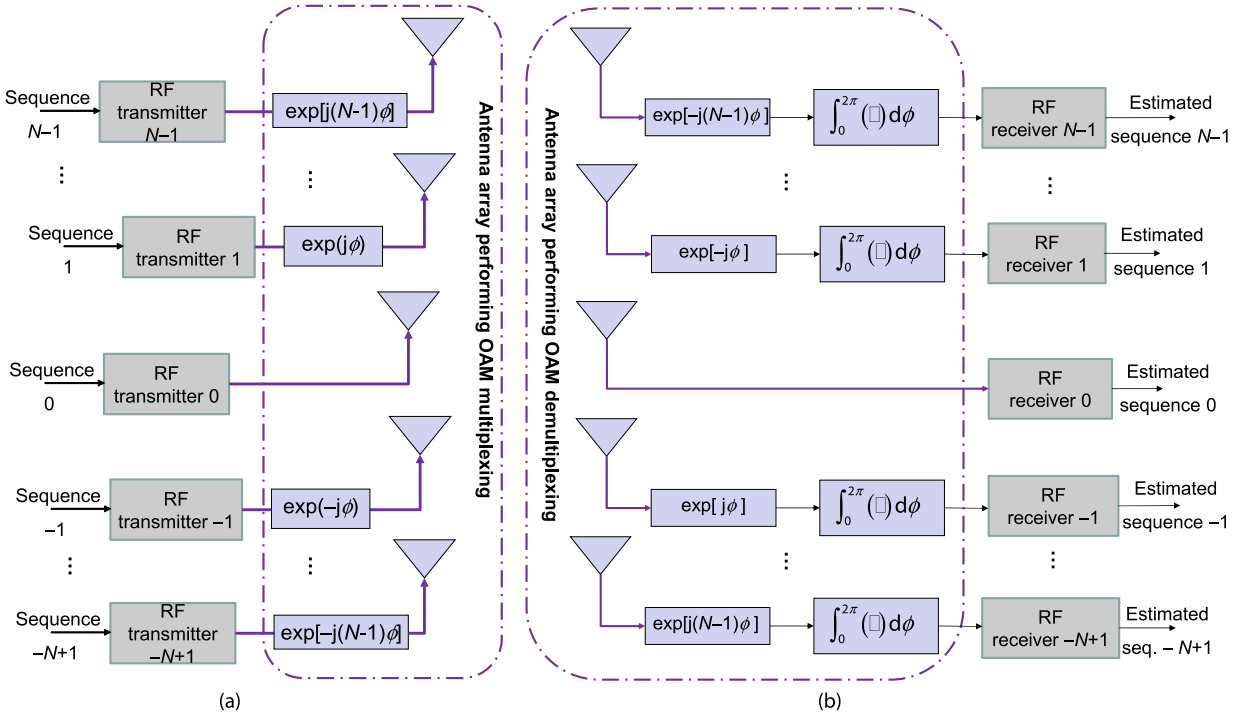

FIGURE 3. Configurations of antenna arrays based: (a) OAM multiplexing and (b) OAM demultiplexing schemes.

multiplexing and demultiplexing are shown in Fig. 3. With the wireless OAM multiplexing we can multiplex $2N + 1$ independent data streams, and therefore improve the spectral efficiency significantly. The energy efficiency can be achieved through optimum signal constellation design and multidimensional signaling that will be described in next section.

Regarding the complexity of proposed RF OAM multiplexer/demultiplexer, compared to traditional antenna array, to impose $(2N + 1)$ OAM modes the use of $(2N + 1)$ SPPs is needed, which can be fabricated by 3-D nanoscribe printer. On the other hand, the spectral efficiency can be improved $(2N + 1)$ times. In the rest of this section we describe how to use OAM in encryption of wireless communication link.

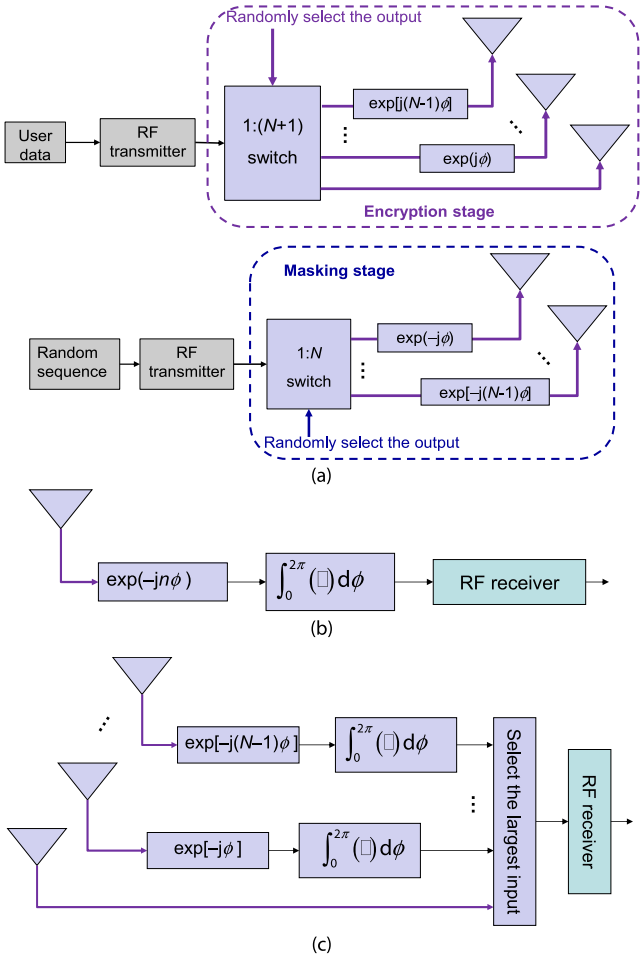

FIGURE 4. OAM-based wireless communication encryption. Configurations of: (a) encryption scheme, (b) decryption scheme, and (c) Eve's apparatus.

B. OAM-BASED ENCRYPTION FOR WIRELESS COMMUNICATIONS APPLICATIONS

In Figure 4 we describe how OAM degree of freedom can be used in wireless communication encryption. The encryption scheme [Fig. 4(a)] is composed of encryption stage and masking stage. In encryption stage, with the help of the switch we randomly select the branch imposing non-negative OAM index basis functions. In masking stage, we randomly select the branch with negative OAM index basis function. In masking stage the samples from complex Gaussian random generator (the LDPC encoder is not needed) are generated. The purpose of this stage is to add the Gaussian noise so that any data structure is lost in both time- and frequency-domains. Since the additive noise is imposed on orthogonal OAM basis function, the de-masking stage is not needed on receiver side. Figure 4(a) represents a conceptual block-diagram. In practice, from implementation point of view, an antenna array in encryption stage will be properly adjusted to generate the randomly selected n-th OAM mode ($n = 0, 1, \ldots, N-1$) to be imposed on transmitted signal. On the other hand, another antenna array is to be used in masking stage to generate randomly selected OAM mode with negative azimuthal mode index, to be imposed on Gaussian noise.

In decryption stage [Fig. 4(b)], the output of antenna array is properly adjusted to detect the desired n-th OAM mode, which is symbolically represented by projection along the n-th OAM basis function. After that, the conventional DT RF receiver, shown in Fig. 2(b), is used to reconstruct the transmitted sequence. Unauthorized user (Eve) will detect the noisy like signal only, since she does not know which OAM index was used. On the other hand, Eve can use apparatus shown in Fig. 4(c) to detect the correct OAM mode. In Eve's apparatus, each element in OAM demultiplexer represents the projection along the OAM basis function with nonnegative OAM indices. Since only one OAM mode is used in encryption stage, only the correct complex conjugate OAM basis function will generate strong peak, the other outputs will generate just noisy signals. Therefore, the circuit selecting the strongest output can be used to identify the correct branch. However, the complexity of Eve's apparatus will be too high for typically required cardinalities in encryption applications.

III. SOFTWARE-DEFINED, ENERGY-EFFICIENT CODED MODULATION (CM) FOR NEXT GENERATION WIRELESS COMMUNICATIONS SYSTEMS

From our previous multidimensional studies, related to optical communications, [7]–[13], we have concluded that the spectral efficiency in multidimensional signaling is a linear function of number of dimensions, while only logarithmic in SNR. Therefore, through multidimensional signaling the spectral efficiency of existing wireless communication systems will be dramatically improved. We first describe the proposed multidimensional coded modulation (CM) scheme suitable for wireless communications.

A. MULTIDIMENSIONAL CM SUITABLE FOR WIRELESS COMMUNICATIONS

The multidimensional DOFs to be utilized include in-phase and quadrature channels, two polarization states, and $(2N+1)$ OAM states, indicating that the resulting signal space is $D = 2 \times 2 \times (2N+1) = 4(2N+1)$-dimensional. Moreover, by replacing the in-phase and quadrature channels by $2L$ baseband basis functions, derived from Slepian sequences, for instance, as we described in [8], [10], and [13], the signal space becomes even $4L(2N+1)$-dimensional. As discussed in [8], [10], and [13], which are related to optical communications, the Slepian sequences $\left\{s_n^{(l)}\left(L_g, W\right)\right\}$ of the l-th order ($l = 0, 1, 2, \ldots$) are mutually orthogonal sequences for sequence length L_g and discrete bandwidth W, and can be determined as a real-valued solution of the following system of discrete equations [33]:

$$\sum_{i=0}^{L_g-1} \{\sin[2\pi\,(n-i)]/[\pi\,(n-i)]\}\, s_i^{(l)}\left(L_g, W\right) = \mu_l\left(L_g, W\right) s_n^{(l)}\left(L_g, W\right) \quad (12)$$

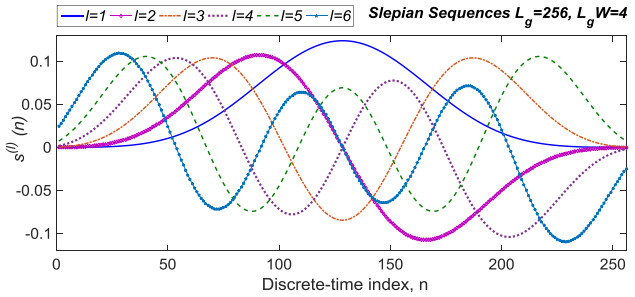

FIGURE 5. Slepian sequences of orders up to six for sequence length of $L_g = 256$.

where i and n denote the particular samples in each Slepian sequence, while the shaping factors $\mu_l(L_g, W)$ are ordered eigenvalues. One of the most important properties of Slepian sequences is the *double orthogonality property*:

$$\begin{aligned}&\sum_{m=0}^{L_g-1} s_m^{(l)}\left(L_g, W\right) s_m^{(k)}\left(L_g, W\right)\\ &\quad = \mu_d\left(L_g, W\right) \sum_{m=-\infty}^{\infty} s_m^{(l)}\left(L_g, W\right) s_m^{(k)}\left(L_g, W\right)\\ &\quad = \mu_d\left(L_g, W\right) \delta_{lk}, \end{aligned} \tag{13}$$

which makes them excellent candidates for wireless communication applications. Namely, given that Slepian sequences stay orthogonal even outside of the desired symbol time-interval, the system based on Slepian sequences is less sensitive to the intersymbol interference (ISI) and multipath fading compared to any other DT basis functions. As an illustration, in Fig. 5 we show the Slepian sequences of order up to 6 to be used as the basis functions, for sequence length of $L_g = 256$. The key idea here is to use the Slepian sequences as either basis functions in baseband domain or as orthogonal impulse responses in passband domain. In baseband domain, the DT basis functions are software-defined, while in passband the gains and phase shifts in antenna array should be properly adjusted so that antenna array will serve as a passband filter with impulse response being a desired Slepian sequence. Therefore, the usage of antenna arrays as the passband filters with impulse responses derived from Slepian sequences can be used as another DOF, which can be called the orthogonal division multiplexing (ODM) DOF, in analogy with corresponding optical communication counterparts [8]–[10], [13]. Now by using K ODM DOFs, the resulting signal space becomes huge, $4LK(2N+1)$-dimensional. As an illustration, by using 12.5 GHz RF carrier, with the help of arbitrary waveform generator (AWG), we can generate 10 Giga symbols/s (GS/s) multidimensional signals, and with wideband antenna arrays to be fabricated with the help of 3-D nanoscribe printer, and for 4-ary signal constellations we can support even $4 \times 4 \times 4 \times (2 \times 2 + 1) \times \log_2(4) \times 10$ GS/s $= 6.4$ Tb/s for small values of $K = L = 4$ and $N = 2$. This indicates that the proposed multidimensional signaling scheme would be multi-Tb/s enabling, and can be used as enabling wireless technology for future 1 Tb/s, 4Tb/s, and 10 Tb/s Ethernets. What is interesting, to achieve such high aggregate data rates, the use of optical communication technologies is not needed at all. Of course, such new wireless technology might require re-allocation of the wireless spectrum, which will be quite challenging. Alternatively, all available U-NII bands should be utilized. For instance, mm-wave and THz bands with center frequencies 85 GHz, 120 GHz, and 250 GHz, have atmospheric attenuations ∼0.5 dB/km, 1 dB/km, and 3 dB/km [34], and as such are excellent candidates for outdoor wireless communications applications as the available bandwidths are comparable to those used in optical wavelength channels. For example, the available bandwidth in 250 GHz range is close to 100 GHz.

Given that 120 GHz technology is becoming commercially available and given that the distances longer than 5 km with data rates of 20 Gb/s have been reported [35], the proposed multidimensional OAM-based coded-modulation scheme represents a promising candidate for the next generation of wireless communication systems. Finally, by employing the cognitive radio concepts [36], the proposed multidimensional wireless communication concepts can be used even with existing wireless spectrum allocation.

To deal with *multipath fading effects*, conventional MIMO approaches can be applied, but instead of 2-D signaling space, the multidimensional signaling space must be used, as follows. Let us consider MIMO system with M_{Tx} transmit array antennas and M_{Rx} receive array antennas, such as those described in previous section. A multidimensional-MIMO channel can be modeled as $\boldsymbol{y} = \boldsymbol{H}\boldsymbol{x} + \boldsymbol{z}$, where $\boldsymbol{x} = [x_1 x_2 \ldots x_{MTx}]^{\mathrm{T}}$ is the transmitted vector, $\boldsymbol{y} = [y_1 y_2 \ldots y_{M\mathrm{Rx}}]^{\mathrm{T}}$ is the received vector, $\boldsymbol{z} = [z_1 \ldots z_{M\mathrm{Rx}}]^{\mathrm{T}}$ is the noise vector, and $\boldsymbol{H}$ is an M_{Rx}-by-M_{Tx} block channel matrix. The i-th element of $\boldsymbol{x}$ is a multidimensional, with each component representing a corresponding basis function from $4LK(2N+1)$-dimensional space, describe above.

The configurations of *2L-dimensional RF modulator and demodulator*, derived from Slepian sequences, discussed earlier, are shown in Fig. 6. To facilitate the explanations, only single polarization state is shown. The $2L$-dimensional RF modulator, shown in Fig. 6(a), generates the signal constellation points as follows:

$$\boldsymbol{x}_i = \sum\nolimits_{l=1}^{L} \boldsymbol{\psi}_{i,l} \boldsymbol{\Psi}^{(l)}, \tag{14}$$

where $\boldsymbol{\psi}_{i,l}$ denotes the l-th complex coordinate ($l = 1, 2, \ldots, L$) of the i-th signal-constellation point, and the set $\{\boldsymbol{\Psi}^{(l)}\}$ denotes the set of the complex basis functions (the real part of each complex basis function corresponds to in-phase channel, while the imaginary part of each complex basis function corresponds to quadrature channel). The $2L$ real Slepian sequences $\{s^{(m)} | m = 1, 2, \ldots, 2L\}$ are used to create the set of DT complex basis functions, with even order sequences corresponding to the real-part and odd order sequences corresponding to the imaginary-parts of these complex basis functions, respectively. Therefore, the

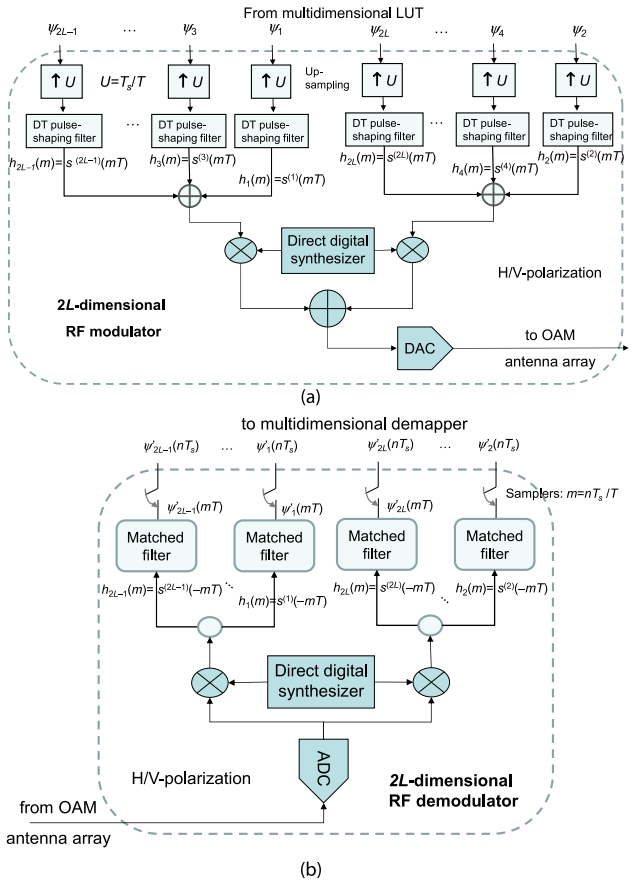

FIGURE 6. Configurations of 2*L*-dimensional RF: (a) modulator and (b) demodulator.

complex set of the basis functions $\{\boldsymbol{\Psi}^{(l)}\}$ has been created from the set of Slepian sequences $\{s^{(m)}\}$ $(m = 1, \ldots, 2L)$ as follows: $\{\boldsymbol{\Psi}^{(l)}\} = \{s^{(2l)} + \mathrm{j}s^{(2l-1)}\}$ $(l = 1, 2, \ldots, L)$. The real-part signal is used as in-phase input, while imaginary-part signal as quadrature input to DT I/Q modulator. The corresponding 2*L*-dimensional RF signal after DAC is used as input to OAM antenna array shown in Fig. 3(a).

On the receiver side, shown in Fig. 6(b), the signal from OAM demultiplexing antenna array [see Fig. 3(b)] is first down-converted to the baseband. The in-phase and quadrature projections represent 2*L*-dimensional baseband signal, and are used as inputs to corresponding matched filters with impulse responses $\boldsymbol{h}_l(n) = \boldsymbol{\Psi}^{*(l)}(-nT)$. Finally, the re-sampled outputs represent projections along the corresponding baseband basis functions, and these projections are used as inputs to the multidimensional *a posteriori* probability (APP) demapper, which calculates symbol log-likelihood ratios (LLRs). The symbol LLRs can be calculated simply by

$$LLR\left(\boldsymbol{x}_i\right) = -\sum\nolimits_{l=1}^{L} \left|\boldsymbol{y}_l - \boldsymbol{x}_{i,l}\right|^2 / 2\sigma^2, \qquad (15)$$

where we use $\boldsymbol{y}_d$ and $\boldsymbol{x}_{i,d}$ to denote the l-th component of received signal constellation point $\boldsymbol{y}$ (along the complex basis function $\boldsymbol{\Psi}^{(l)}$ and transmitted symbol $\boldsymbol{x}_i$, respectively; while σ^2 is the variance of an equivalent noise upon detection. Therefore, even for large number of coordinates the symbol LLRs are easy to calculate for Gaussian noise dominated wireless channels.

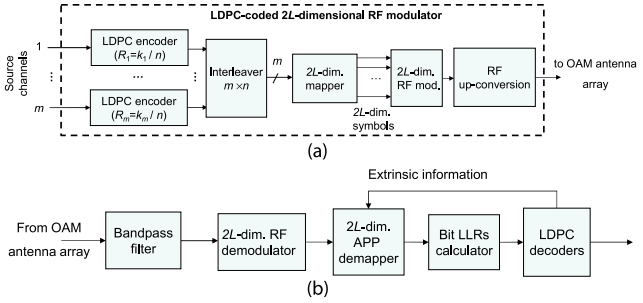

FIGURE 7. Configurations of adaptive software-defined: (a) LDPC-coded 2*L*-dimensional RF modulator and (b) 2*L*-dimensional iterative APP demapper-LDPC decoding.

The proposed multidimensional coded modulation scheme is flexible. It can be used to multiplex different 2*L*-dimensional streams, in similar fashion as shown in Fig. 3 with corresponding RF transmitter and receiver configurations shown in Fig. 7, to fully $4LK(2N + 1)$-dimensional signaling. In adaptive, software-defined, LDPC coded modulation scheme (see Fig. 7), the independent data streams are LDPC encoded, and corresponding codewords are written into interleaver. The code rates are adapted based on time-varying multipath channel conditions. From interleaver, m bits are taken at each symbol interval and used to select a point from 2*L*-dimensional signal constellation, with coordinates written into a look-up-table (LUT). These coordinates are imposed on different DT basis functions derived from Slepian sequences, as shown in Fig. 6(a). The up-conversion block is needed for frequency division multiplexing (FDM).

With a help of OAM antenna array [see Fig. 3(a)], such obtained multidimensional signal is imposed on a desired OAM mode. On receiver side, the outputs of receive OAM antenna array [see Fig. 3(b)] will provide the projections along corresponding OAM basis functions. Each OAM demultiplexer output will be passed through the bandpass filter to select the desired frequency band, then in 2*L*-dimensional demodulator, shown in Fig. 6(b), we will obtain the projections along baseband DT basis functions, and these projections will be forwarded to 2*L*-dimensional APP demapper [see Fig. 6(b)] to calculate the symbol LLRs, according to Eqn. (15). In bit LLRs calculator, we calculate bit LLRs to be used in binary LDPC decoders, as described in [37]. We will then iterate extrinsic information between LDPC decoders and APP demapper to improve the overall BER performance. Various coded modulation (CM) concepts [37]–[45] can be applied to the proposed multidimensional CM, including the multilevel coding (MLC) [37], [38], [40], [45]. Finally, the nonbinary MLC in which component codes are LDPC codes over GF(4) are interesting in particular, given that this approach is not sensitive to the

mapping rule as shown in [37]. The channel capacity achieving modulation formats can also be used [37], [46], [47], together with optimal mapping rules [37].

As an illustration, the iterative polar modulation (IPM) based on iterative polar quantization (IPQ) has been introduced in [46]. It is well known that for a Gaussian noise dominated channel model, the optimum information source is Gaussian. This indicates that the optimum signal constellation contains constellation points placed on circles that follow Rayleigh radius distribution. Recently, we extended this signal constellation design to multidimensional signal space, and corresponding signal constellation design was named optimized vector-quantization-inspired signal constellation design (OVQ-SCD) in [9]. For smaller constellation sizes, the optimum signal constellation design (OSCD) was advocated in [47]. Given that these multidimensional signal constellation designs are maximizing the mutual information for AWGN, they will be employed later in Section V. However, these designs do not take the energy constrains into account, which is the subject of the next subsection.

B. ENERGY-EFFICIENT SIGNAL CONSTELLATION DESIGN FOR WIRELESS COMMUNICATION APPLICATIONS

Energy-efficient coded modulation can be achieved through efficient signal constellation design, while taking the energy constraint into account. Below we will describe a generic approach for providing energy-efficient constellation. The problem can be formulated as follows. Consider a set of multidimensional symbols $X = \{x_1, x_2, \ldots, x_M\}$ that occur with *a priori* probabilities $p_1, \ldots, p_M$, where $p_i = \Pr(x_i)$. Let the corresponding symbol energies be $E_1, \ldots, E_M$. These symbols are to be transmitted over the wireless communication link. We require that $\sum_i p_i E_i \leq E$ (an energy constraint). In the presence of noise and various channel impairments, we can use the Lagrangian method to maximize the mutual information $I(X, Y)$, defined as $I(X, Y) = H(X) - H(X|Y)$, where $H(X)$ is the entropy of the channel input X and $H(X|Y)$ is the conditional entropy of X given the channel output Y. Taking the energy constraint into account, the corresponding Lagrangian $\mathscr{L}$ will be:

$$\mathscr{L} = \overbrace{-\sum_i p_i \log p_i}^{H(X)} - \overbrace{(-\sum_i p_i \sum_j P_{ij} \log Q_{ji})}^{H(X|Y)} + \eta\left(\sum_i p_i - 1\right) + \mu\left(\sum_i p_i E_i - E\right) \tag{16}$$

where $P_{ij} = \Pr(y_j|x_i)$ denotes the transitional probabilities, determined through channel estimation, and $Q_{ji} = \Pr(x_i|y_j)$, which can be determined by Bayes' rule as $Q_{ji} = \Pr(x_i|y_j) = \Pr(x_i, y_j)/\Pr(y_j) = P_{ij}p_i/\sum_k P_{kj}p_k$. The optimum signal constellation coordinates cannot be found in analytical form. However, we can use the following *energy-efficient signal-constellation design* (EE-SCD) algorithm, similar to [12], to obtain a near-optimal result:

1) *Initialization*: Choose an arbitrary auxiliary input distribution and signal constellation, where the number of constellation points M_{aux} is much larger than the target signal constellation M. For a uniform distribution, $p_i = 1/M_{aux}$.
   a) Q_{ji} *update-rule*:
   $$Q_{ji}^{(t)} = P_{ij}p_i^{(t)} / \sum_k P_{kj}p_k^{(t)}.$$
   b) p_i *update-rule*:
   $$p_i^{(t+1)} = e^{-\mu E_i - H^{(t)}(x_i|Y)} / \sum_k e^{-\mu E_k - H^{(t)}(x_k|Y)},$$
   where the Lagrange multiplier μ is determined from the energy constraint.
2) The constellation points of the target constellation are obtained as the *center of mass* of the closest M_{aux}/M constellation points in the auxiliary signal constellation.

Steps 1)-3) are repeated until the algorithm reaches the convergence. Well-known Arimoto-Blahut algorithm [48] does not impose an energy constraint, and yields the optimum source distribution only. Using EE-SCDA, we can obtain the optimized signal constellation while taking the energy constraint into account. Both optimum source distribution and EE signal constellation are obtained from this algorithm. This algorithm should be applied to various wireless channel conditions, before transmission takes place, and corresponding results should be stored in multidimensional LUTs, implemented in FPGA/ASIC hardware. Based on predominant channel conditions, during transmission, corresponding LUT, storing the coordinates of a multidimensional constellation, will be activated. On such a way, all complexities related to EE-SCD will be solved in the installation stage.

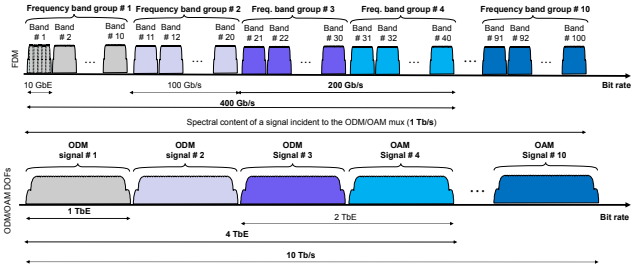

FIGURE 8. Four-levels of multiplexing-based digital hierarchy enabling up to 10 Tb/s wireless communication.

C. DIGITAL HIERARCHY ENABLING BEYOND 1 Tb/s AGGREGATE DATA RATES FOR WIRELESS APPLICATIONS

To provide *fine granularity in wireless spectrum utilization*, four levels of multiplexing can be used: two levels of FDM, ODM, and OAM-multiplexing, as illustrated in Fig. 8. Such approach enables proper multiplexing of many wireless channels to reach even beyond 1 Tb/s serial data rates. First two levels of multiplexing will be multiband-OFDM based, in similar fashion as it has been already proposed for optical

communications [9], [13]. In this particular example, we assume that 3 ODM DOFs and 7 RF OAM modes are used. The starting point is 10 Gb/s wireless signal originating either from 10 GbE or 10 data streams of rates 1 Gb/s get RF multiplexed firsts into 10 Gb/s band i ($i = 1, 2, \ldots, 100$) signal. The center frequencies of bands within the band group are mutual orthogonal frequencies. The center frequencies of the band groups are mutually orthogonal as well. This approach is quite flexible as the aggregate data rate can be varied from 1 Gb/s to 10 Tb/s. When multi-Tb/s data rates are not needed, the second level of FDM can be omitted.

IV. PHYSICAL-LAYER SECURITY FOR MULTIDIMENSIONAL WIRELESS COMMUNICATION SYSTEMS

In addition to the encryption scheme described in subsection II.B, three types of PLS schemes are applicable here: classical, semi-classical, and quantum; depending on the desired level of security. It is well-known that classical protocols rely on the computational difficulty of reversing the one-way functions [49], [50], and in principle cannot provide any indication of Eve's presence at any point in the communication process. However, the wireless communication links can be operated at a desired margin from the receiver sensitivity, defined as the minimum required receive antenna power to achieve the target BER, and for known channel conditions the Eve's presence can be detected as it will cause sudden decrease in *secrecy capacity* C_s, defined as $C_s = C_{AB} - C_{AE}$ where C_{AB} is the instantaneous capacity of Alice-Bob channel and C_{AE} is the instantaneous capacity of Alice-Eve channel. Regarding the classical case, OAM DOF is used to multiplex independent streams so that secrecy capacity can be linearly increased with the number of DOFs. From our recent studies of spatial division multiplexing (SDM) systems, such as [7]–[13]; we have learned that channel capacity can be increased linearly with number of spatial modes, rather than logarithmically with SNR for conventional 2-D schemes. This observations motivates us to employ the OAM wireless modes to dramatically improve secrecy capacity when compared to conventional 2-D schemes. For AWGN channel in the presence of fading, the instantaneous secrecy capacity for two polarization states, $(2N + 1)$ OAM modes, and K ODM DOFs is given by:

$$C_s = 2K\,(2N+1)\left[\log_2\left(1+\gamma_{AB}\right) - \log_2\left(1+\gamma_{AE}\right)\right]^+, \tag{17}$$

where we use $[x]^+$ to denote $\max(0, x)$. In (17) γ_{AB} (γ_{AE}) denotes the SNR in Alice-Bob (Alice-Eve) channel. Clearly, the secrecy capacity is a linear function in number of OAM modes and ODM DOFs; in other words, quadratic in proposed DOFs. The use of OAM-based schemes to increase the secret key rates is always sensitive to the crosstalk among OAM modes and potential eavesdropper can compromise the security by relying on OAM modes coupling, without being detected by Alice and Bob. To solve for this problem, we propose not only to compensate for coupling among OAM/ODM modes, but also to rely on multidimensional signaling. In multidimensional signaling, the OAM modes and Slepian sequences can be used as basis functions, and by detecting the signal in any particular DOF Eve will not be able to compromise security as only a single coordinate will be detected. Since the multidimensional signaling in wireless communications has been already described earlier, here we just briefly describe the corresponding multidimensional scheme to be used for raw key transmission over heterogeneous wireless links, which is based on Figs. 3 and 7. The configurations of multidimensional modulator and demodulator, OAM multiplexer and demultiplexer, are already provided in our previous section. Alice generates the binary sequence randomly. The multidimensional mapper can be implemented as an LUT. For signal constellation size M, $m = \log_2 M$ bits are used to find the coordinates of multidimensional signal constellation, obtained as we have described previously. The multidimensional coordinates are used as the inputs to corresponding multidimensional RF modulator. After the OAM-multiplexing, the signal is transmitted over wireless communication system of interest. On receiver side, after OAM-demultiplexing, down-conversion, and multidimensional demodulation, the estimated multidimensional coordinates are used as inputs of multidimensional APP demapper, which provides the most probably symbol being transmitted, and the detected sequence is delivered to Bob. After that information reconciliation, based on systematic LDPC coding, is performed in similar fashion as already proposed for QKD applications [51]. To distill from the generated key a smaller set of bits whose correlation with Eve's string falls below the desired threshold, the privacy amplification [52] is performed with the help of the *universal hash functions*.

For users concerned with unconditional security we propose to use hybrid RF-free-space-optical (FSO) continuous variable quantum key distribution (CV-QKD) as we described in [53].

V. ILLUSTRATIVE NUMERICAL RESULTS

To demonstrate high potential of the proposed multidimensional coded modulation scheme, suitable for wireless communications, we perform Monte Carlo simulations over generalized fading channels. In particular, the α-μ fading model is employed because Rayleigh, Nakagami-m, exponential, Weibull and one-sided Gaussian distribution functions, to mention few, are all special cases of α-μ distribution [54]. The corresponding α-μ probability density function (PDF) of envelope r is given by [54]

$$f_R(r) = \frac{\alpha\mu^{\mu} r^{\alpha\mu-1}}{\hat{r}^{\alpha\mu}\Gamma(\mu)} \exp\left(-\mu\frac{r^{\alpha}}{\hat{r}^{\alpha}}\right), \tag{18}$$

where $\Gamma(\cdot)$ is the Gamma function and $\hat{r}$ is a α-root mean value $\hat{r} = \langle r^{\alpha}\rangle^{1/\alpha}$, with $\langle\cdot\rangle$ being the expectation operator. As an illustration, by setting $\alpha = 2$ and $\mu = 1$ we obtain the Rayleigh distribution, while by setting $\alpha = 2$ and $\mu = 2$

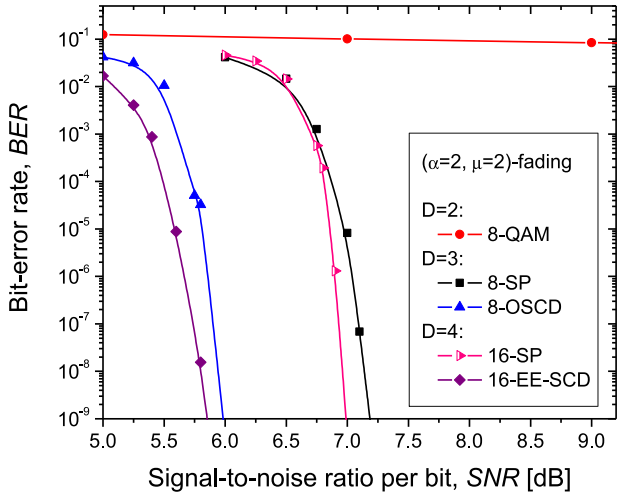

FIGURE 9. BER vs. bit SNR for different LDPC (16935, 13550)-coded modulation schemes of dimensionalities 2, 3, and 4 in the presence of Nakagami $m = 2$, ($\alpha = 2$, $\mu = 2$), fading.

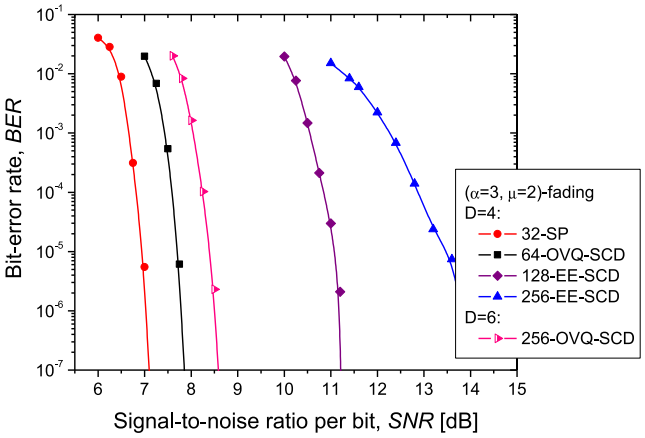

FIGURE 10. BER vs. bit SNR for different LDPC (16935, 13550)-coded modulation schemes of dimensionalities 4 and 6 in the presence of ($\alpha = 3$, $\mu = 2$) fading.

we obtain Nakagami $m = 2$ distribution. The corresponding PDF of SNR γ is given by:

$$f_\Gamma(\gamma) = \frac{\alpha \mu^\mu}{2\bar{\gamma}^{\alpha\mu/2}\Gamma(\mu)} \gamma^{\frac{\alpha\mu}{2}-1} \exp\left[-\mu\left(\frac{\gamma}{\bar{\gamma}}\right)^{\alpha/2}\right], \quad (19)$$

where $\bar{\gamma}$ is the average SNR.

As an illustration of high potential of proposed OAM-based multidimensional coded modulation, suitable for wireless communication applications, in Fig. 9 we show bit-error rate (BER) plots for various 8-ary and 16-ary LPDC-coded modulation schemes for dimensionality D ranging from 2 to 4, in the presence of Nakagami $m = 2$ fading ($\alpha = 2$, $\mu = 2$).

The bit-interleaved LDPC-coded modulation with parallel dependent decoding is employed, as described in [55]. In simulations, the quasi-cyclic LDPC (16935, 13550) code of code rate 0.8, girth 8, and column-weight 3 is used. The number of outer APP-demapper LDPC decoders is set to 4,

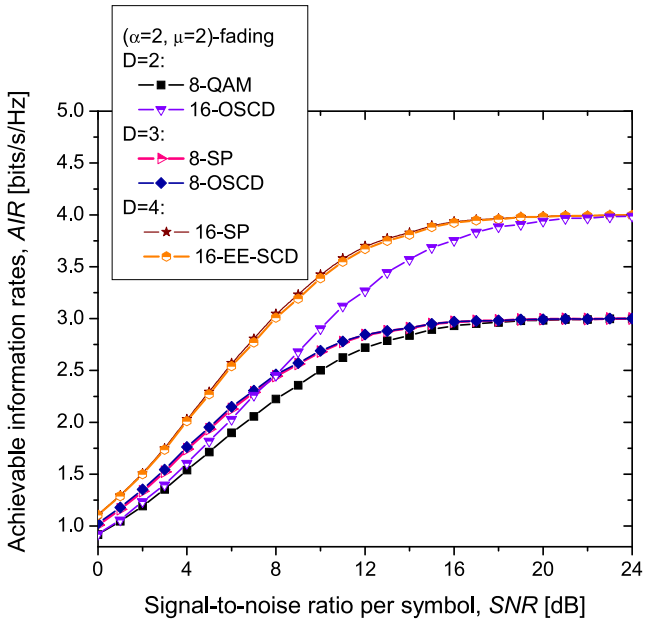

FIGURE 11. Ergodic achievable information rates vs. symbol SNR for different modulation schemes of dimensionalities 2, 3, and 4 in the presence of Nakagami $m = 2$, ($\alpha = 2$, $\mu = 2$), fading.

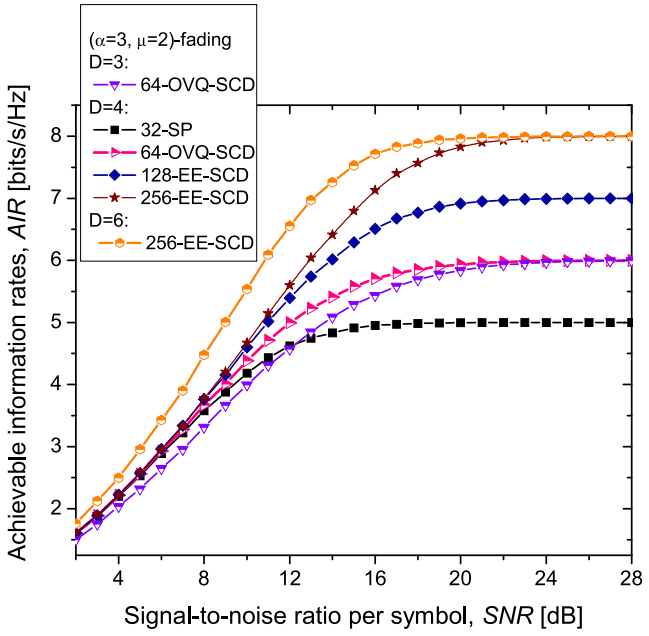

FIGURE 12. Ergodic achievable information rates vs. symbol SNR for different modulation schemes of dimensionalities 3, 4, and 6 in the presence of ($\alpha = 3$, $\mu = 2$) fading.

while the number of inner (LDPC decoder) iterations is set to 25. What is interesting to notice is that LDPC-coded 8-QAM cannot be used at all in Nakagami-2 fading in single-input single-output (SISO) configuration, while schemes of dimensionality 3 and constellation size 8 do not exhibit any error floor phenomenon down to 10^{-9}. The LDPC-coded 16-ary 4-D constellation obtained by EE-SCD, described

in subsection III.B outperforms the LDPC-coded sphere-packing (SP) constellation [56] by 1.16 dB at BER of 10^{-8}.

In Figure 10 we show BER vs. bit SNR performance of various LDPC-coded modulations schemes of dimensionalities 4 and 6 in ($\alpha = 3$, $\mu = 2$)-fading. Clearly, in order to improve the tolerance to fading effects, we need to increase dimensionality of the system. Based on these numerical results, we can conclude the tolerance to fading effects can be improved by increasing of dimensionality of the system instead of applying the diversity and MIMO signal processing approaches. Moreover, by employing the proposed digital hierarchy (see subsection III.C), multi-Tb/s wireless communication is possible by using the proposed multidimensional coded modulation scheme.

Corresponding achievable information rates (AIRs), calculated in similar fashion as described in [57], of various multidimensional modulation schemes in the presence of (α, μ)-fading are summarized in Figs. 11-12. As expected, the increase in dimensionality improves the tolerance to generalized fading effects.

VI. CONCLUDING REMARKS

The key challenges for beyond 5G wireless technologies are quite difficult to solve simultaneously with currently existing wireless networks technologies. To solve for these problems, it necessary to make a dramatic improvement in both wireless spectrum and energy efficiencies in order to cope with the incoming bandwidth capacity crunch. Moreover, the security issues in wireless networks are not adequately addressed, and new approaches are needed to address the physical-layer security problems.

To address these key challenges for future beyond 5G wireless technologies in a simultaneous manner, in this paper, we have proposed to employ the OAM-based, secured, energy-efficient multidimensional coded modulation scheme suitable for high-speed wireless communications. The main idea followed in this paper has been to use all available DOFs to convey the information over the wireless links including amplitude, phase, polarization state, and OAM modes. In particular, given that the OAM is associated with azimuthal phase dependence of the wavefront, wherein eigenstates are mutually orthogonal, an arbitrary number of bits per symbol can be transmitted. Additionally, the Slepian sequences have been employed twofold: (i) as the baseband basis functions and (ii) as the impulse responses of properly designed antenna arrays. The performed Monte Carlo simulations have demonstrated high tolerance to fading effects of the proposed multidimensional coded modulation scheme. Further, we have proposed the wireless encryption scheme based on OAM modes. A digital hierarchy has been proposed as well employing various DOFs listed above, combined with multidimensional signaling, enabling multi-Tb/s wireless transmission. Finally, the multidimensional physical-layer security scheme has been proposed with the secrecy capacity being a linear function in number of OAM modes and linear function in number of ODM DOFs, dramatically improving the secrecy capacities of conventional 2-D modulation schemes.

REFERENCES

[1] P. Demestichas *et al.*, "5G on the horizon: Key challenges for the radio-access network," *IEEE Veh. Technol. Mag.*, vol. 8, no. 3, pp. 47–53, Sep. 2013.

[2] E. Hossain and M. Hasan, "5G cellular: Key enabling technologies and research challenges," *IEEE Instrum. Meas. Mag.*, vol. 18, no. 3, pp. 11–21, Jun. 2015.

[3] A. Hakiri and P. Berthou, "Leveraging SDN for the 5G networks: Trends, prospects and challenges," in *Software Defined Mobile Networks: Beyond LTE Network Architecture* (Series in Communications Networking and Distributed Systems). Hoboken, NJ, USA: Wiley, Jun. 2015, pp. 1–23.

[4] M. R. Palattella *et al.*, "Internet of Things in the 5G era: Enablers, architecture, and business models," *IEEE J. Sel. Areas Commun.*, vol. 34, no. 3, pp. 510–527, Mar. 2016.

[5] T. Rossi, M. De Sanctis, E. Cianca, C. Fragale, M. Ruggieri, and H. Fenech, "Future space-based communications infrastructures based on high throughput satellites and software defined networking," in *Proc. IEEE Int. Symp. Syst. Eng.*, Sep. 2015, pp. 332–337.

[6] L. Cheng, M. Zhu, M. M. U. Gul, X. Ma, and G.-K. Chang, "Adaptive photonics-aided coordinated multipoint transmissions for next-generation mobile fronthaul," *J. Lightw. Technol.*, vol. 32, no. 10, pp. 1907–1914, May 1, 2014.

[7] I. B. Djordjevic, M. Arabaci, L. Xu, and T. Wang, "Spatial-domain-based multidimensional modulation for multi-Tb/s serial optical transmission," *Opt. Exp.*, vol. 19, no. 7, pp. 6845–6857, Mar. 2011.

[8] I. B. Djordjevic, M. Cvijetic, and C. Lin, "Multidimensional signaling and coding enabling multi-Tb/s optical transport and networking," *IEEE Signal Process. Mag.*, vol. 31, no. 2, pp. 104–117, Mar. 2014.

[9] I. B. Djordjevic, A. Jovanovic, Z. H. Peric, and T. Wang, "Multidimensional optical transport based on optimized vector-quantization-inspired signal constellation design," *IEEE Trans. Commun.*, vol. 62, no. 9, pp. 3262–3273, Sep. 2014.

[10] I. B. Djordjevic, A. H. Saleh, and F. Kueppers, "Design of DPSS based fiber Bragg gratings and their application in all-optical encryption, OCDMA, optical steganography, and orthogonal-division multiplexing," *Opt. Exp.*, vol. 22, no. 9, pp. 10882–10889, May 2014.

[11] I. B. Djordjevic, "Energy-efficient spatial-domain-based hybrid multidimensional coded-modulations enabling multi-Tb/s optical transport," *Opt. Exp.*, vol. 19, no. 17, pp. 16708–16714, Aug. 2011.

[12] I. B. Djordjevic, L. Xu, and T. Wang, "Statistical physics inspired energy-efficient coded-modulation for optical communications," *Opt. Lett.*, vol. 37, no. 8, pp. 1340–1342, Apr. 2012.

[13] I. B. Djordjevic, "On the irregular nonbinary QC-LDPC-coded hybrid multidimensional OSCD-modulation enabling beyond 100 Tb/s optical transport," *J. Lightw. Technol.*, vol. 31, no. 16, pp. 2969–2975, Aug. 15, 2013.

[14] L. Allen, M. W. Beijersbergen, R. J. C. Spreeuw, and J. P. Woerdman, "Orbital angular-momentum of light and the transformation of Laguerre-Gaussian laser modes," *Phys. Rev. A*, vol. 45, pp. 8185–8189, Jun. 1992.

[15] G. Gibson *et al.*, "Free-space information transfer using light beams carrying orbital angular momentum," *Opt. Exp.*, vol. 12, no. 22, pp. 5448–5456, 2004.

[16] I. B. Djordjevic and M. Arabaci, "LDPC-coded orbital angular momentum (OAM) modulation for free-space optical communication," *Opt. Exp.*, vol. 18, no. 24, pp. 24722–24728, 2010.

[17] N. Bozinovic, S. Golowich, P. Kristensen, and S. Ramachandran, "Control of orbital angular momentum of light with optical fibers," *Opt. Lett.*, vol. 37, no. 13, pp. 2451–2453, Jul. 2012.

[18] N. Bozinovic *et al.*, "Terabit-scale orbital angular momentum mode division multiplexing in fibers," *Science*, vol. 340, pp. 1545–1548, Jun. 2013.

[19] Z. Qu and I. B. Djordjevic, "500Gb/s free-space optical transmission over strong atmospheric turbulence channels," *Opt. Lett.*, vol. 41, no. 14, pp. 3285–3288, Jul. 2016.

[20] I. B. Djordjevic and Z. Qu, "Coded orbital angular momentum modulation and multiplexing enabling ultra-high-speed free-space optical transmission," in *Optical Wireless Communications—An Emerging Technology*, M. Uysal, C. Capsoni, Z. Ghassemlooy, A. Boucouvalas, and E. G. Udvary, Eds. Cham, Switzerland: Springer, 2016.

[21] I. B. Djordjevic and Z. Qu, "Coded orbital-angular-momentum-based free-space optical transmission," in *Encyclopedia of Electrical and Electronics Engineering*. Hoboken, NJ, USA: Wiley, Feb. 2016.
[22] I. B. Djordjevic, J. A. Anguita, and B. Vasic, "Error-correction coded orbital-angular-momentum modulation for FSO channels affected by turbulence," *J. Lightw. Technol.*, vol. 30, no. 17, pp. 2846–2852, Sep. 1, 2012.
[23] X. Sun and I. B. Djordjevic, "Physical-layer security in orbital angular momentum multiplexing free-space optical communications," *IEEE Photon. J.*, vol. 8, no. 1, pp. 01110-1–01110-10, Feb. 2016, doi: 10.1109/JPHOT.2016.2519279.
[24] I. B. Djordjevic and X. Sun, "Spatial modes-based physical-layer security," in *Proc. IEEE ICTON*, Jul. 2016, pp. 1–5.
[25] S. Zheng, X. Hui, X. Jin, H. Chi, and X. Zhang, "Transmission characteristics of a twisted radio wave based on circular traveling-wave antenna," *IEEE Trans. Antennas Propag.*, vol. 63, no. 4, pp. 1530–1536, Apr. 2015.
[26] F. Tamburini *et al.*, "Encoding many channels on the same frequency through radio vorticity: First experimental test," *New J. Phys.*, vol. 14, pp. 033001–033017, Mar. 2012.
[27] X. Hui *et al.*, "Multiplexed millimeter wave communication with dual orbital angular momentum (OAM) mode antennas," *Sci. Rep.*, vol. 5, p. 10148, May 2015.
[28] B. Thidé *et al.*, "Utilization of photon orbital angular momentum in the low-frequency radio domain," *Phys. Rev. Lett.*, vol. 99, p. 087701, Aug. 2007.
[29] Q. Bai, A. Tennant, and B. Allen, "Experimental circular phased array for generating OAM radio beams," *Electron. Lett.*, vol. 50, pp. 1414–1415, Aug. 2004.
[30] A. Willner, Y. Yan, Y. Ren, N. Ahmed, and G. Xie, "Orbital angular momentum-based wireless communications: Designs and implementations," in *Signal Processing for 5G: Algorithms and Implementations*, F.-L. Luo and C. Zhang, Eds. Chichester, U.K.: Wiley, 2005, pp. 296–318.
[31] C. A. Balanis, *Antenna Theory: Analysis and Design*, 4th ed. Hoboken, NJ, USA: Wiley, 2016.
[32] S. Verdú, *Multiuser Detection*. New York, NY, USA: Cambridge Univ. Press, 1998.
[33] D. Slepian, "Prolate spheroidal wave functions, Fourier analysis, and uncertainty—V: The discrete case," *Bell Syst. Tech. J.*, vol. 57, no. 5, pp. 1373–1381, 1978.
[34] A. V. Räisänen *et al.*, "Propagation at THz frequencies," in *Semiconductor Terahertz Technology: Devices and Systems at Room Temperature Operation*, G. Carpintero, L. E. G. Munoz, H. L. Hartnagel, S. Preu, and A. V. Räisänen, Eds. Hoboken, NJ, USA: Wiley, 2015, pp. 160–211.
[35] T. Nagatsuma, "THz communication systems," in *Proc. OFC*, Mar. 2017, pp. 19–23 .
[36] E. Biglieri, A. J. Goldsmith, L. J. Greenstein, N. B. Mandayam, and H. V. Poor, *Principles of Cognitive Radio*. Cambridge, U.K.: Cambridge Univ. Press, 2013.
[37] I. B. Djordjevic, "On advanced FEC and coded modulation for ultra-high-speed optical transmission," *IEEE Commun. Surveys Tuts.*, vol. 18, no. 3, pp. 1920–1951, 3rd Quart., 2016, doi: 10.1109/COMST.2016.2536726.
[38] H. Imai and S. Hirakawa, "A new multilevel coding method using error correcting codes," *IEEE Trans. Inf. Theory*, vol. IT-23, no. 3, pp. 371–377, May 1977.
[39] G. Ungerboeck, "Channel coding with multilevel/phase signals," *IEEE Trans. Inf. Theory*, vol. IT-28, no. 1, pp. 55–67, Jan. 1982.
[40] U. Wachsmann, R. F. H. Fischer, and J. B. Huber, "Multilevel codes: Theoretical concepts and practical design rules," *IEEE Trans. Inf. Theory*, vol. 45, no. 5, pp. 1361–1391, Jul. 1999.
[41] K. R. Narayanan and J. Li, "Bandwidth efficient low density parity check codes using multilevel coding and iterative multistage decoding," in *Proc. 2nd Symp. Turbo Codes Rel. Top.*, Brest, France, 2000, pp. 165–168.
[42] S. Benedetto, D. Divsalar, G. Montorsi, and H. Pollara, "Parallel concatenated trellis coded modulation," in *Proc. IEEE Int. Conf. Commun.*, Dallas, TX, USA, Jun. 1996, pp. 974–978.
[43] G. Caire, G. Taricco, and E. Biglieri, "Bit-interleaved coded modulation," *IEEE Trans. Inf. Theory*, vol. 44, no. 3, pp. 927–946, May 1998.
[44] J. Tan and G. L. Stuber, "Analysis and design of symbol mappers for iteratively decoded BICM," *IEEE Trans. Wireless Commun.*, vol. 4, no. 2, pp. 662–672, Mar. 2005.
[45] J. Hou, P. H. Siegel, L. B. Milstein, and H. D. Pfister, "Capacity-approaching bandwidth-efficient coded modulation schemes based on low-density parity-check codes," *IEEE Trans. Inf. Theory*, vol. 49, no. 9, pp. 2141–2155, Sep. 2003.
[46] I. B. Djordjevic, H. G. Batshon, L. Xu, and T. Wang, "Coded polarization-multiplexed iterative polar modulation (PM-IPM) for beyond 400 Gb/s serial optical transmission," in *Proc. OFC/NFOEC*, 2010, pp. 21–25.
[47] T. Liu and I. B. Djordjevic, "Multidimensional optimal signal constellation sets and symbol mappings for block-interleaved coded-modulation enabling ultrahigh-speed optical transport," *IEEE Photon. J.*, vol. 6, no. 4, Aug. 2014, Art. no. 5500714.
[48] R. E. Blahut, "Computation of channel capacity and rate distortion functions," *IEEE Trans. Inf. Theory*, vol. IT-18, no. 7, pp. 460–473, Jul. 1972.
[49] M. Bloch, J. Barros, M. R. D. Rodrigues, and S. W. McLaughlin, "Wireless information-theoretic security," *IEEE Trans. Inf. Theory*, vol. 54, no. 6, pp. 2515–2534, Jun. 2008.
[50] I. B. Djordjevic, *Quantum Information Processing and Quantum Error Correction: An Engineering Approach*. San Francisco, CA, USA: Academic, Apr. 2012.
[51] I. B. Djordjevic, "Integrated optics modules based proposal for quantum information processing, teleportation, QKD, and quantum error correction employing photon angular momentum," *IEEE Photon. J.*, vol. 8, no. 1, pp. 6600212-1–6600212-12, Feb. 2016.
[52] C. H. Bennett, G. Brassard, C. Crépeau, and U. M. Maurer, "Generalized privacy amplification," *IEEE Trans. Inf. Theory*, vol. 41, no. 6, pp. 1915–1923, Nov. 1995.
[53] Z. Qu and I. B. Djordjevic, "High-speed free-space optical continuous-variable quantum key distribution enabled by three-dimensional multiplexing," *Opt. Exp.*, vol. 25, no. 7, pp. 7919–7928, 2017.
[54] M. D. Yacoub, "The α-μ distribution: A physical fading model for the Stacy distribution," *IEEE Trans. Veh. Technol.*, vol. 56, no. 1, pp. 27–34, Jan. 2007.
[55] D. Zou, C. Lin, and I. B. Djordjevic, "FPGA-based LDPC-coded APSK for optical communication systems," *Opt. Exp.*, vol. 25, no. 4, pp. 3133–3142, Feb. 2017.
[56] N. J. A. Sloane, R. H. Hardin, T. D. S. Duff, and J. H. Conway, "Minimal-energy clusters of hard spheres," *Discrete Comput. Geometry*, vol. 14, no. 3, pp. 237–259, 1995.
[57] I. B. Djordjevic, "LDPC-coded MIMO optical communication over the atmospheric turbulence channel using Q-ary pulse-position modulation," *Opt. Exp.*, vol. 15, no. 16, pp. 10026–10032, Aug. 2007.

IVAN B. DJORDJEVIC (M'05–SM'11) was with the University of Bristol and the University of the West of England, Bristol, U.K.; Tyco Telecommunications, Eatontown, USA; the National Technical University of Athens, Athens, Greece; and State Telecommunication Company, Nis, Yugoslavia. He is currently a tenured Professor with the ECE Department, College of Engineering, The University of Arizona, with a joint appointment in the College of Optical Sciences. He has authored or co-authored five books, over 450 international journal/conference publications, and 40 U.S. patents. Prof. Djordjevic is an OSA Fellow. He serves as an Associate Editor for five journals.